Chemical Science

ROYAL SOCIETY OF CHEMISTRY

EDGE ARTICLE

View Article Online
View Journal | View Issue

Cite this: *Chem. Sci.*, 2023, **14**, 1461

All publication charges for this article have been paid for by the Royal Society of Chemistry

Received 3rd December 2022
Accepted 12th January 2023

DOI: 10.1039/d2sc06675k

rsc.li/chemical-science

A mitochondria-localized iridium(III) photosensitizer for two-photon photodynamic immunotherapy against melanoma†

Lili Wang,[ae] Johannes Karges,[b] Fangmian Wei,[a] Lina Xie,[a] Zhuoli Chen,[a] Gilles Gasser,*[c] Liangnian Ji[a] and Hui Chao*[ad]

Conventional photodynamic therapy mainly causes a therapeutic effect on the primary tumor through the localized generation of reactive oxygen species, while metastatic tumors remain poorly affected. Complementary immunotherapy is effective in eliminating small, non-localized tumors distributed across multiple organs. Here, we report the Ir(III) complex Ir-pbt-Bpa as a highly potent immunogenic cell death inducing photosensitizer for two-photon photodynamic immunotherapy against melanoma. Ir-pbt-Bpa can produce singlet oxygen and superoxide anion radicals upon light irradiation, causing cell death by a combination of ferroptosis and immunogenic cell death. In a mouse model with two physically separated melanoma tumors, although only one of the primary tumors was irradiated, a strong tumor reduction of both tumors was observed. Upon irradiation, Ir-pbt-Bpa not only induced the immune response of $CD8^+$ T cells and the depletion of regulatory T cells, but also caused an increase in the number of the effector memory T cells to achieve long-term anti-tumor immunity.

Introduction

Melanoma is an aggressive form of skin cancer that occurs when pigment-generating cells mutate into cancerous cells. Based on its high drug resistance, fast tumor relapse, and high capacity for the development of metastases, this form of cancer remains a clinical challenge.[1] Clinically applied methods to treat this cancer rely on surgery, chemotherapy, and radiotherapy.[2–4] Studies have demonstrated that photodynamic therapy (PDT) shows only poor therapeutic efficacy against melanoma.[5] Since PDT is ideal for treating skin diseases due to its superficiality, it would be of high interest to modify this therapeutic method to allow its application against melanoma.[6]

PDT has been associated with three interconnected mechanisms: (1) production of reactive oxygen species (ROS) in the tumor; (2) damage of the vasculature to deprive the tumor of oxygen and nutrients; (3) induction of an inflammatory reaction that can activate the host immune system.[7–9] Recently, much attention has been devoted to the combination of these mechanisms through the localized generation of oxidative stress and the systemic induction of an immune response inside the organism by immunogenic cell death (ICD).[10–12] This form of cell death is typically triggered through the generation of oxidative stress in the mitochondria or the endoplasmic reticulum (ER).[13] Through the translocation of calreticulin, the release of adenosine triphosphate (ATP), and the migration of the high-mobility group box 1 (HMGB1) protein, cancer cells can release damage-associated molecular patterns (DAMPs) that can subsequently induce the maturation of dendritic cells and therefore activate the systemic antitumor immune response.[14]

The majority of currently studied photosensitizers are based on a tetrapyrrolic scaffold that is usually but not always associated with several limitations such as (1) poor (photo-) stability,[15,16] (2) low water solubility,[17] and (3) poor absorption in the near-infrared region,[9,18] making the application of these compounds for PDT not ideal.[11] It was shown that the subcellular localization (*e.g.*, mitochondria, endoplasmic reticulum, and lysosome) of the photosensitizer is crucial in an immunogenic response.[19] A majority of studied photosensitizers do not localize in these cell organelles, resulting in a relatively scarce number of compounds, which can therapeutically intervene by ICD.[20]

[a]*MOE Key Laboratory of Bioinorganic and Synthetic Chemistry, School of Chemistry, Guangdong Provincial Key Laboratory of Digestive Cancer Research, The Seventh Affiliated Hospital, Sun Yat-Sen University, Guangzhou, 510006, P. R. China. E-mail: ceschh@mail.sysu.edu.cn*

[b]*Faculty of Chemistry and Biochemistry, Ruhr-University Bochum, Universitätsstrasse 150, 44780 Bochum, Germany*

[c]*Chimie ParisTech, PSL University, CNRS, Institute of Chemistry for Life and Health Sciences, Laboratory for Inorganic Chemical Biology, Paris, 75005, France. E-mail: gilles.gasser@chimieparistech.psl.eu*

[d]*MOE Key Laboratory of Theoretical Organic Chemistry and Functional Molecule, School of Chemistry and Chemical Engineering, Hunan University of Science and Technology, Xiangtan, 400201, P. R. China*

[e]*Public Research Center, Hainan Medical University, Haikou, 571199, P. R. China*

† Electronic supplementary information (ESI) available. See DOI: https://doi.org/10.1039/d2sc06675k

Increasing research efforts have been devoted to the application of metal complexes as ICD-inducing photosensitizers due to their high (photo-)stability, efficient ROS production, facile synthesis, and easy tuneability for precise subcellular targeting.[21–25] To date, these endeavors for photodynamic immunotherapy have been focused on compounds based on Pt(IV), Ru(II), Ir(III), and Re(I).[14,26–28] Brabec and co-workers reported on a Pt(IV) prodrug that could be reduced into the respective Pt(II) species upon irradiation, causing the release of damage-associated molecular patterns and cell death by ICD.[29] Karges and Xiao described the incorporation of Pt(IV) complexes into the backbone of polymeric nanoparticles. Upon excitation, the Pt(IV) center was selectively reduced to Pt(II) and the nanomaterial dissociated, causing cell death by ICD.[30] The McFarland group reported on Ru(II) complexes that could catalytically generate singlet oxygen upon light irradiation, triggering cell death by ICD.[7] Mao and co-workers prepared a carbonic anhydrase IX anchored Re(I) complex that could induce the maturation of dendritic cells and cause cell death through a combination of pyroptosis and ICD upon exposure to light.[31] The research groups of Ruiz and Brabec reported on an Ir(III) complex that could generate ROS upon light irradiation and cause oxidative stress in melanoma cells, triggering cell death by ICD.[32] Despite these primary studies, the reported metal complexes were usually associated with a poor immunological response and/or poor excitation in the near-infrared region, limiting the application of these compounds.

In an effort to shift the excitation window into the near-infrared region, much research efforts have been focused on the design of photosensitizers for two-photon PDT.[33] Among the evaluated metal complexes, cyclometalated Ir(III) complexes have emerged as novel agents with ideal properties for two-photon PDT (*i.e.*, strong two-photon absorption, strong luminescence, high ROS production, and high stability).[34,35] Previous studies have shown that the two-photon absorption properties[36–38] as well as the excited state lifetime and ROS production[37,39] could be enhanced upon extension of the aromatic conjugated ligand scaffold.

Capitalizing on these preliminary studies, herein, the nature of the previously reported chemotherapeutic agent Ir-Bpa, which does not induce ICD,[40] was changed to an ICD-inducing photosensitizer for two-photon excited photodynamic immunotherapy by replacement of the ancillary ligand 2-phenylpyridine to 2-phenylbenzo[*d*]-thiazole Ir-pbt-Bpa (Fig. 1). The extension of the aromatic system was found to enhance the two-photon absorption, the ROS production, as well as changed the primary subcellular target from the ER to the mitochondria. Upon excitation with one- or two-photon light, Ir-pbt-Bpa was found to effectively produce singlet oxygen, superoxide anion radicals, and lipid peroxides, ultimately leading to cell death in melanoma cancer cells by a combination of ferroptosis and ICD. The biological properties of Ir-pbt-Bpa were further studied in an animal model with a primary and distant melanoma tumor. While the compound and light were only administered to the primary tumor, a strong reduction of the primary and the distant tumor was observed. Immunogenic studies inside the animal model indicated the enhanced maturation of dendritic cells, the inhibition of the tumor immunosuppressive

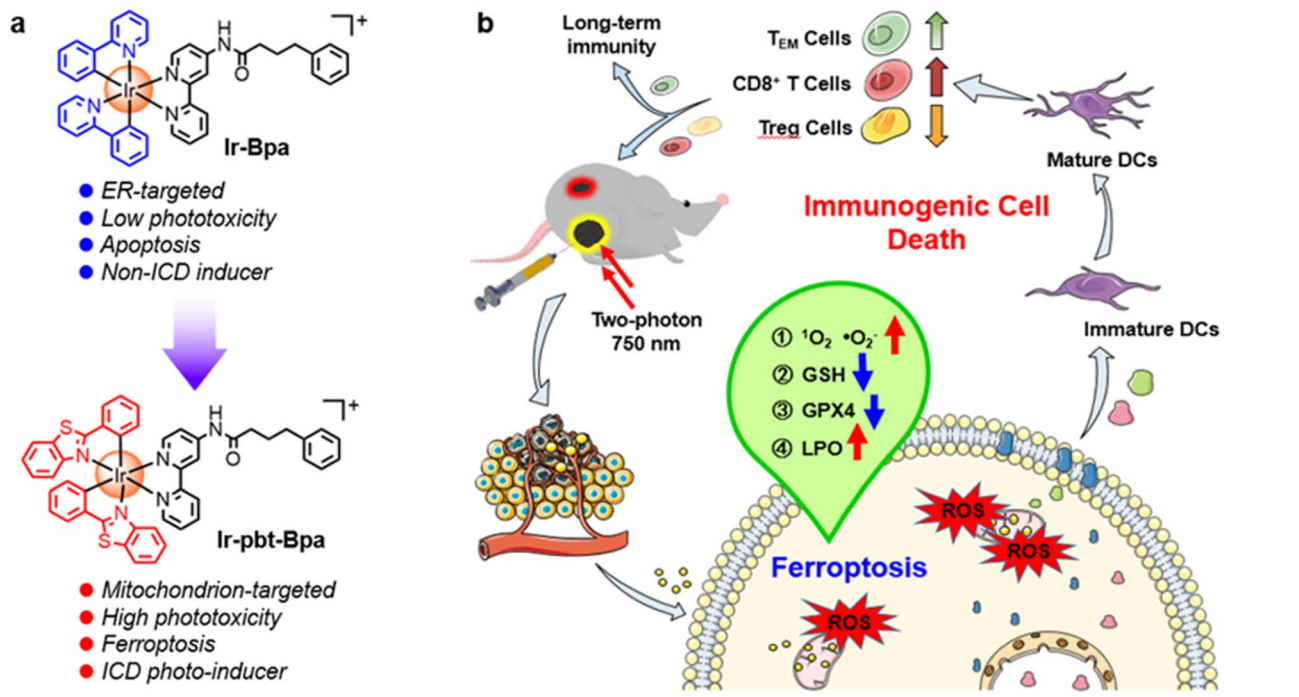

Fig. 1 Schematic illustration of the Ir(III) photosensitizer for two-photon photodynamic immunotherapy against melanoma. (a) Schematic illustration of the structures and properties of Ir-Bpa and Ir-pbt-Bpa. (b) Mechanism of action of Ir-pbt-Bpa as a photosensitizer for two-photon photodynamic immunotherapy in melanoma cancer cells.

microenvironment, and the generation of long-lasting memory immune cells. To the best of our knowledge, this study reports on the first example of an iridium-based two-photon excited photosensitizer, which triggers cell death by ICD. This photosensitizer could therefore find application for photodynamic immunotherapy.

Results and discussion

Synthesis and characterization

The cyclometalated Ir(III) complexes Ir-pbt-Bpa and Ir-Bpa were synthesized as described in the experimental section (Scheme S1†). The metal complexes were characterized by electrospray ionization mass spectrometry and proton nuclear magnetic resonance spectroscopy and their purity was checked by HPLC (Fig. S1 and 2†). Ir-pbt-Bpa exhibited a strong absorption band at 300–350 nm with an absorption tail reaching approximately 500 nm (Fig. S3a†). To ensure the treatment of deep-seated tumors, photosensitizers with excitation in the near-infrared region are sought. Among the applied strategies to ensure excitation in this region, the use of two-photon PDT is receiving increasing attention.[36] Despite preliminary studies, the majority of currently studied photosensitizers are associated with poor two-photon absorption, rendering the application of these compounds not ideal although it is only one of the necessary characteristics for a good therapeutic outcome.[41] The metal complexes Ir-Bpa and Ir-pbt-Bpa were found to have a two-photon absorption from 740–800 nm (Fig. S4†). The absorption maximum was detected at 750 nm with a two-photon absorption cross-section of 75 GM for Ir-pbt-Bpa and 5 GM for Ir-Bpa (1 GM = 10^{-50} cm^4 s^{-1} photon^{-1}). Upon excitation, Ir-pbt-Bpa demonstrated a strong emission centered at 580 nm (Fig. S3b†). The photostability of Ir-pbt-Bpa was assessed upon continuous irradiation at 405 nm in CD_3CN and monitoring of the potential conversion of the compound by electrospray ionization mass spectrometry and proton nuclear magnetic resonance spectroscopy (Fig. S5 and 6†). Promisingly, no changes were observed, indicative of the high photostability of Ir-pbt-Bpa and Ir-Bpa. Moreover, the stability of Ir-pbt-Bpa in FBS was also confirmed by HPLC (Fig. S7†).

The ability of the metal complexes to catalytically generate singlet oxygen upon excitation at 405 nm was quantified upon time-dependent monitoring of the conversion of 1,3-diphenyliso-benzofuran. Ir-Bpa was found to have a singlet oxygen quantum yield of 0.23 and Ir-pbt-Bpa of 0.35 in methanol (Fig. S8†). The potential generation of types of ROS was investigated by electron spin resonance spectroscopy using the singlet oxygen scavenger 2,2,6,6-tetramethylpiperidine and the superoxide anion radicals radical scavenger 5,5-dimethyl-1-pyrroline *N*-oxide. In agreement with the previous assessment, a stronger triplet signal corresponding to (2,2,6,6-tetramethylpiperidin-1-yl)oxyl was observed for Ir-pbt-Bpa than Ir-Bpa upon irradiation (Fig. S9†). While the solution of Ir-Bpa did not show any signal upon incubation with 5,5-dimethyl-1-pyrroline *N*-oxide, a characteristic but weak signal corresponding to the formation of superoxide anion radicals upon irradiation of Ir-pbt-Bpa was detected (Fig. S10†). We speculate that the inclusion of heterocycles may facilitate spin-orbital coupling and thus enhance inter-system crossing, which results in higher photosensitizing efficiency.

(Photo-)cytotoxicity *in vitro*

The toxicity of Ir-Bpa and Ir-pbt-Bpa in the dark as well as upon irradiation (405 nm, 0.75 J cm^{-2}) was studied against human and murine versions of breast cancer (MDA-MB-231, 4T1), lung cancer (A549, LLC), colon cancer (SW620, CT-26), and melanoma (A375, B16F10) cells. Both metal complexes were found to be relatively cytotoxic in the dark in the micromolar range (Ir-Bpa: $IC_{50,dark}$ = 6.7–15.2 μM, Ir-pbt-Bpa: $IC_{50,dark}$ = 3.2–22.0 μM), which may be attributed to the ability of the compounds to generate ROS in the dark (Fig. 2c). Upon irradiation, the compounds were able to generate ROS more efficiently and therefore cause a phototoxic effect (Ir-Bpa: $IC_{50,light}$ = 1.0–5.0 μM, Ir-pbt-Bpa: $IC_{50,light}$ = 0.4–1.4 μM). The comparison between the dark and light toxicity values, namely the photo-index, shows that Ir-pbt-Bpa has a better safety profile than Ir-Bpa. Ir-pbt-Bpa demonstrated the strongest therapeutic effect on breast cancer and melanoma cells (Table S1†), although the photo indexes are rather low. For verification of the (photo-) toxic effect, treated A375 cells (Fig. 2f) and B16F10 cells (Fig. S11†) were stained with the cell live/dead markers calcein-am/propidium iodide. While the majority of cells remained alive upon treatment in the dark, a large amount of cell death was observed upon exposure of the treated cells to light.

Intracellular uptake and subcellular localization

The subcellular localization of Ir-pbt-Bpa in A375 cells was studied by confocal laser scanning microscopy. The microscopy images showed a high congruency with Pearson's correlation coefficient (PCC) of 0.84 with the mitochondria-specific dye Mito Tracker™ Red (Fig. 2a), indicating mitochondria as the primary localization of the metal complex. For a deeper understanding of the subcellular distribution, the iridium content inside the major cellular organelles was investigated by inductively coupled plasma mass spectrometry. The complex was found to be primarily localizing in the mitochondria (Fig. 2b). Due to the change in subcellular localization, the lipophilicities (log *P*) were determined for the compounds. Ir-Bpa was found to have a log *P* value of 1.1 and Ir-pbt-Bpa of 0.8 (Fig. S12†). We speculate that the change in subcellular localization of the compound might be related to the decrease in the lipophilicity of the compound.

Intracellular ROS, Ca^{2+}, and ER stress levels

Studies have shown that tumor regression can be promoted by inducing progressive mitochondrial and endoplasmic reticulum damage and irreversible ER stress. ROS is thought to play a critical role in fuelling this vicious cycle.[42] To investigate the ability of Ir-pbt-Bpa to generate ROS inside cancer cells, A375 cells were co-incubated with the ROS-specific probe dichlorodihydrofluorescein diacetate, and the generation of ROS monitored by flow cytometry. While some amounts of ROS were produced upon treatment with Ir-pbt-Bpa in the dark,

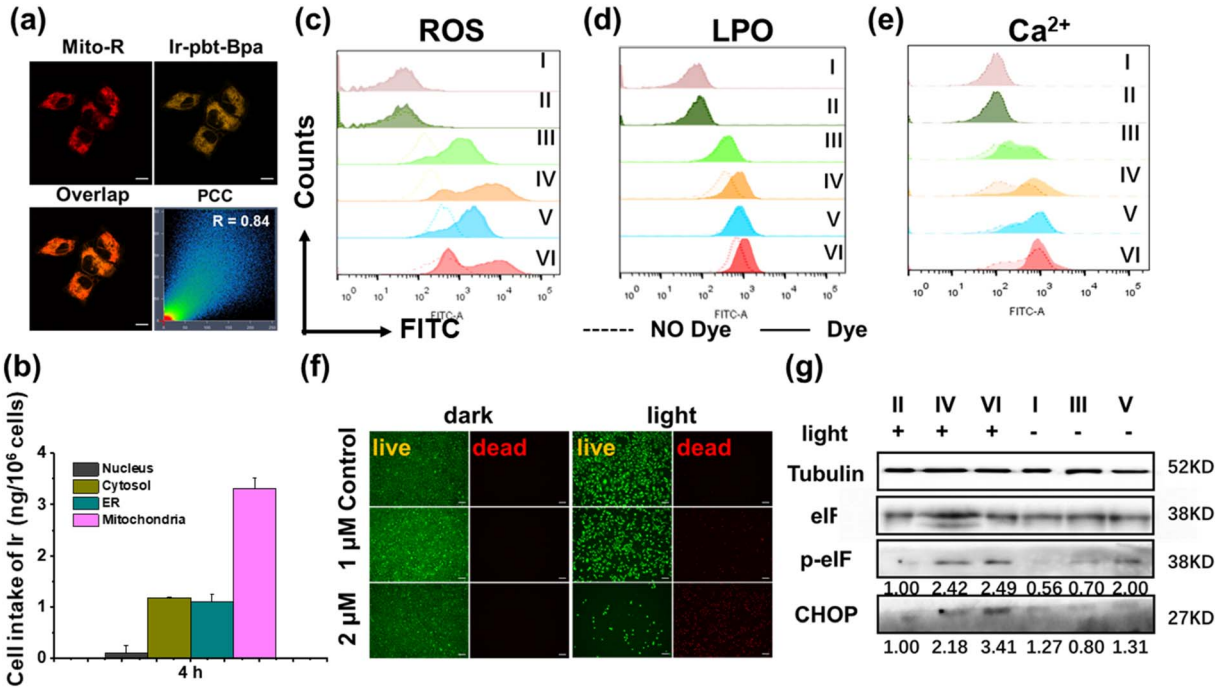

Fig. 2 Cellular localization and photocytotoxicity. (a) Confocal laser scanning microscopy images of A375 cells upon incubation with Ir-pbt-Bpa (2 μM) for 4 h and MitoTracker™ Red (Mito-R) for 0.5 h. Scale bar: 10 μm. (b) Subcellular distribution of Ir-pbt-Bpa (2 μM) upon incubation in A375 cells for 4 h determined by inductively coupled plasma mass spectrometry. Flow cytometry spectrum upon treatment of A375 cells with Ir-pbt-Bpa to investigate the ability of the compound to (c) generate ROS, (d) produce lipid peroxides or (e) release Ca^{2+} ions. (I) Cells were kept in the dark; (II) cells were exposed to irradiation (405 nm LED, 0.75 J cm^{-2}); (III) cells were incubated with Ir-pbt-Bpa (concentration: IC_{50} value) for 4 h in the dark, (IV) cells were incubated with Ir-pbt-Bpa (concentration: 2× IC_{50} value) for 4 h in the dark; (V) cells were incubated with Ir-pbt-Bpa (concentration: IC_{50} value) for 4 h and exposed to irradiation (405 nm LED, 0.75 J cm^{-2}), (IV) cells were incubated with Ir-pbt-Bpa (concentration: 2× IC_{50} value) for 4 h and exposed to irradiation (405 nm LED, 0.75 J cm^{-2}). The dashed lines represent the negative controls without dye. (f) Fluorescence microscopy images of A375 cells upon incubation with Ir-pbt-Bpa for 4 h and calcein-AM (live, green)/propidium iodide (dead, red) in the dark or upon irradiation (405 nm LED, 0.75 J cm^{-2}). Scale bar: 100 μm. (g) Image of the western blot analysis of the treatment of A375 cells with Ir-pbt-Bpa. (I) cells were kept in the dark; (II) cells were exposed to irradiation (405 nm LED, 0.75 J cm^{-2}); (III) cells were incubated with Ir-pbt-Bpa (1 μM) for 4 h in the dark, (IV) cells were incubated with Ir-pbt-Bpa (1 μM) for 4 h and exposed to irradiation (405 nm LED, 0.75 J cm^{-2}), (V) cells were incubated with Ir-pbt-Bpa (2 μM) for 4 h in the dark; (IV) cells were incubated with Ir-pbt-Bpa (2 μM) for 4 h and exposed to irradiation (405 nm LED, 0.75 J cm^{-2}).

a significant enhancement of the ROS generation was observed upon exposure to light (Fig. 2c). Similar behavior was detected in B16F10 cells (Fig. S13†). As expected, the fluorescence of dichlorofluorescein (DCF) was significantly enhanced for Ir-pbt-Bpa after two-photon ($\lambda_{ex} = 750$ nm) irradiation (Fig. S14†). The production of oxidative stress in the mitochondria was recently found to be ideal for the generation of multimodal therapeutic agents.[43,44] Capitalizing on this, the possible generation of ER stress upon treatment with Ir-pbt-Bpa was studied upon determination of the levels of the C/EBP homologous protein (CHOP) and the phosphorylation of eukaryotic initiation factor 2α (p-eIF2α) by western blot analysis. An increased expression of CHOP and p-eIF2α in A375 cells and B16F10 cells was observed (Fig. 2g and S15†), indicative of ER stress during the treatment. In addition, as a signature hallmark event of ICD, the extracellular exposure of DAMPs originates from the activation of ER stress.[45–49] Previous studies have suggested that ER stress could lead to the loss of the ER membrane integrity and therefore the release of Ca^{2+} ions.[50] To investigate this, the fluorophore Fluo-4 AM was co-incubated with the cancer cells, and the change in fluorescence was monitored by flow cytometry. The release of Ca^{2+} ions from the ER into the cytoplasm upon treatment with Ir-pbt-Bpa could be demonstrated (Fig. 2e and S16†).

Ferroptosis

Ferroptosis is a newly discovered form of cell death caused by the accumulation of iron-dependent lipid peroxides (LPOs)[51–53] that has recently been associated with immune responses in tumors.[54–56] Several studies have even described ferroptosis cell death as a form of ICD.[57,58] Ferroptosis is considered a complex process that is associated with the consumption of glutathione, decreased expression of glutathione peroxidase 4 (GPX4), and the generation of LPOs.[59,60] Capitalizing on this, the treatment of A375 cells with Ir-pbt-Bpa was investigated towards these ferroptosis-specific hallmarks. While the glutathione-disulfide/glutathione ratio did not significantly change upon treatment with Ir-pbt-Bpa in the dark, a strong enhancement upon exposure to light was monitored (Fig. S17†), indicating the depletion of glutathione. As glutathione is the natural substrate of GPX4, previous studies have indicated that the consumption of

glutathione could inhibit the expression of GPX4.[61] Using western blot analysis, the decreased expression of GPX4 upon treatment with Ir-pbt-Bpa and exposure to light was confirmed (Fig. S18†). Followingly, the production of LPOs during the treatment was studied by flow cytometry using the Image-iT® Lipid Peroxidation Kit. While some amount of LPO was produced upon treatment with Ir-pbt-Bpa in the dark, a significant enhancement of the LPO generation was observed upon exposure to light in A375 and B16F10 cells (Fig. 2d and S19†). Using confocal laser scanning microscopy, the LPO generation in A375 and B16F10 cells were visualized (Fig. S20 and 21†). Furthermore, the fluorescence of LPO was only observed for Ir-pbt- Bpa after two-photon ($\lambda_{ex} = 750$ nm) irradiation (Fig. S22†). The combination of these findings indicated that the treatment with Ir-pbt-Bpa and exposure to light irradiation likely causes cell death by ferroptosis.

For an understanding of the contribution of ferroptosis in comparison to traditional cell death mechanism, A375 cells were pre-treated with apoptosis (Z-VAD-FMK), necrosis (necrostatin-1), and ferroptosis (ferrostatin-1) inhibitors and the cell survival monitored. While the pre-incubation with ferroptosis inhibitors did strongly enhance cell survival during the treatment with Ir-pbt-Bpa and exposure to irradiation, the pre-incubation with apoptosis and necrosis inhibitors seemed to be ineffective (Fig. S23†). These results indicate that the metal complex does not trigger cell death by apoptosis or necrosis but mainly induces ferroptosis.

Hallmarks of ICD in cells and multicellular tumor spheroids (MCTS)

As previous studies have indicated that ferroptosis cell death could be associated with ICD, the influence of the metal

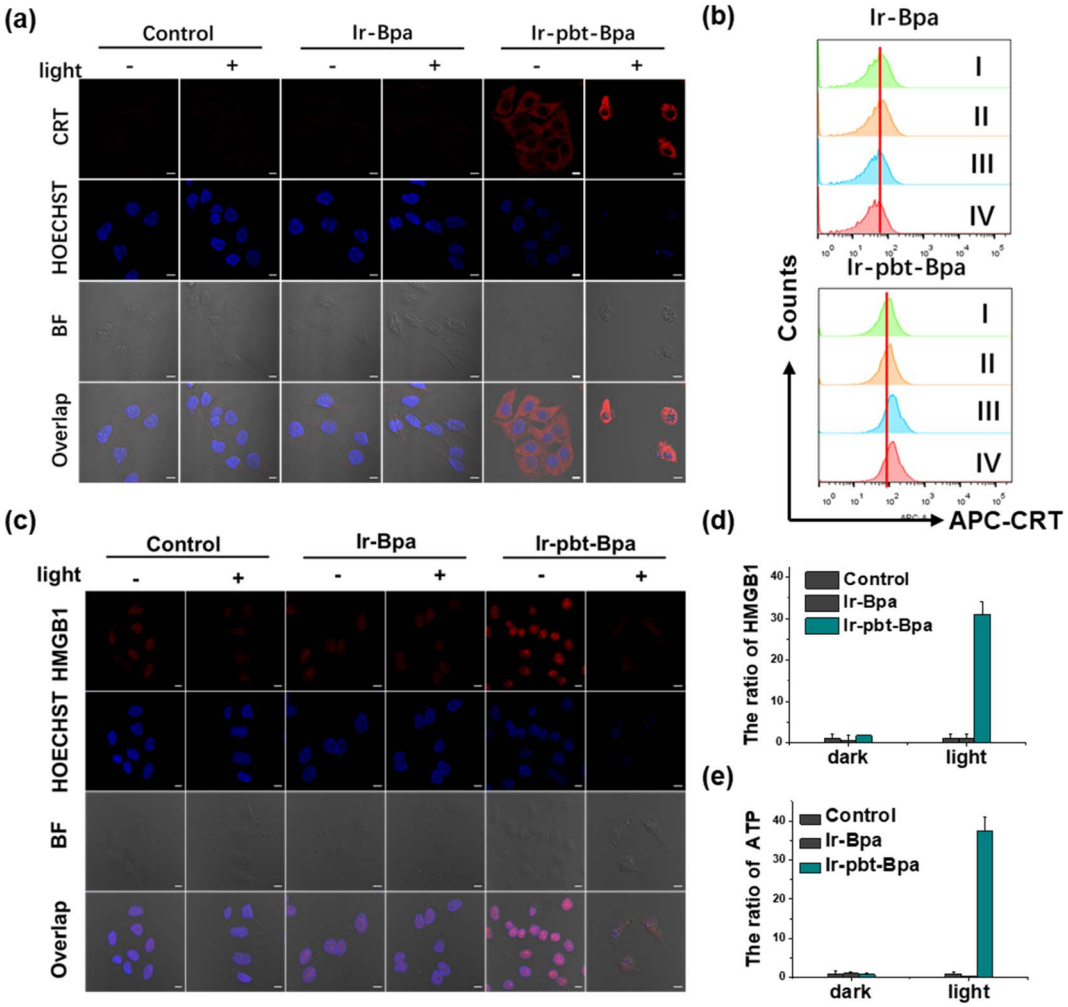

Fig. 3 Evaluation for hallmarks of ICD in A375 cells. Evaluation for hallmarks of ICD in A375 cells upon treatment with Ir-Bpa (1 μM) and Ir-pbt-Bpa (1 μM) in the dark or upon irradiation (405 nm LED, 0.75 J cm^{-2}). (a) Immunofluorescence confocal laser scanning microscopy stained with a calreticulin-specific antibody. Scale bar: 10 μm. (b) Flow cytometry spectrum to investigate the translocation of calreticulin. (I) cells were kept in the dark; (II) cells were exposed to irradiation (405 nm LED, 0.75 J cm^{-2}); (III) cells were incubated with Ir-pbt-Bpa (1 μM) for 4 h in the dark, (IV) cells were incubated with Ir-pbt-Bpa (1 μM) for 4 h and exposed to irradiation (405 nm LED, 0.75 J cm^{-2}). (c) Immunofluorescence confocal laser scanning microscopy stained with a nuclear high-mobility group box 1 protein-specific antibody. Scale bar: 10 μm. (d) Release of nuclear high-mobility group box 1 protein into the cell culture supernatant. (e) Release of adenosine triphosphate into the cell culture supernatant.

complex on this form of cell death was studied.[62] This mechanism involves the translocation of the ER-resident calreticulin and heat shock protein 70 (HSP70) to the cell surface, the secretion of adenosine triphosphate (ATP), and the secretion of the nuclear high-mobility group box 1 (HMGB1) protein. These hallmarks were therefore investigated upon treatment of A375 cells with Ir-pbt-Bpa. Using immunofluorescence confocal laser scanning microscopy, the translocation of calreticulin was observed. No changes upon treatment with Ir-Bpa in the dark or light were observed. In comparison, a significant amount of calreticulin was observed in the cytoplasm or the cell membrane upon treatment with Ir-pbt-Bpa in the dark or upon irradiation (Fig. 3a). These findings were further confirmed by flow cytometry (Fig. 3b). Using immunofluorescence confocal laser scanning microscopy, the possible migration of HMGB1 was monitored. No changes in the localization of HMGB1 upon treatment with Ir-Bpa were observed. On the contrary, the nuclear HMGB1 protein migrated from the nucleus into the extracellular space upon treatment with Ir-pbt-Bpa upon irradiation (Fig. 3c). The extracellular release of HMGB1 to the supernatant was quantified by an ELISA assay. An approximately 31-fold enhancement of extracellular levels of HMGB1 was found upon treatment and exposure to light (Fig. 3d). Surface-exposure of HSP70 was also confirmed by confocal microscopy (Fig. S24†). Followingly, the extracellular secretion of ATP was studied using a specific bioluminescence detection kit. A 37-fold enhancement of the extracellular ATP levels upon treatment of the cancer cells with Ir-pbt-Bpa and exposure to irradiation was observed (Fig. 3e). Furthermore, there were also significant differences in the amount of HMGB1 and ATP released by Ir-pbt-Bpa towards A375 cells in the dark and under different illumination powers (0.75 J cm^{-2}, 1.5 J cm^{-2}, 3 J cm^{-2}). Significant reductions in the levels of HMGB1 and ATP were observed upon enhancement of the light doses, indicative of 0.75 J cm^{-2} as the preferred irradiation conditions (Fig. S25 and 26, Table S2†). The combination of these findings indicates that Ir-pbt-Bpa can trigger ICD upon light irradiation. Besides the evaluation in A375 cells, Ir-pbt-Bpa was also found to trigger ICD in B16F10 cells (Fig. S27–31†).

Following the evaluation in monolayer cells, the biological properties of our new complexes were further studied in MCTS. MCTS can better simulate the tumor characteristics by taking the penetration of extracellular barriers, proliferation gradients, or hypoxia into consideration. Using one- and two-photon excited z-stack confocal laser scanning microscopy, the ability of Ir-pbt-Bpa to penetrate the cell architecture of A375 MCTS was investigated. As luminescence signals were detected at every section depth, the complete penetration of the MCTS with Ir-pbt-Bpa is indicated (Fig. 4a). It is important to mention that the NIR two-photon irradiation is able to penetrate significantly deeper into the tissue than upon exposure to blue one-photon light. To investigate the ability to cause a phototoxic effect upon two-photon irradiation, A375 MCTS were incubated with Ir-pbt-Bpa and exposed to two-photon light (750 nm, 50 mW). The metal complex was found to have a phototoxic effect in the micromolar range ($IC_{50,dark}$ = 25.8 μM, $IC_{50,light}$ = 4.9 μM) (Table S3†). The (photo-)toxic effect was verified upon staining of the MCTS with the cell live/dead markers calcein-am/propidium iodide. The MCTS showed a large amount of cell death upon treatment and exposure to light (Fig. S32†). Based

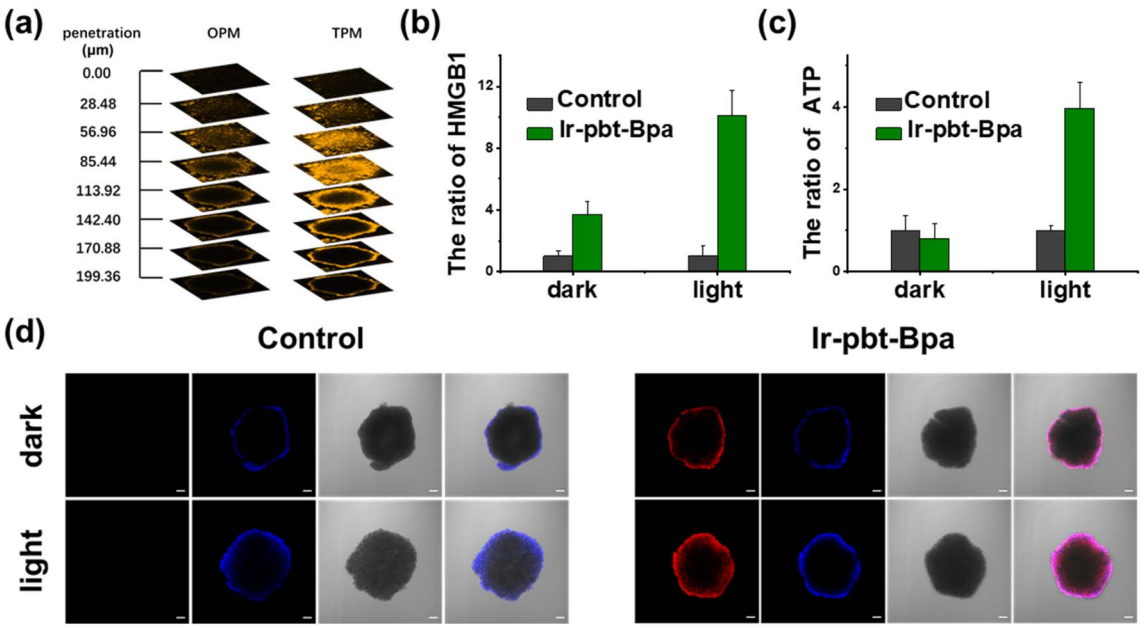

Fig. 4 Evaluation for hallmarks of ICD in A375 MCTS. Evaluation for hallmarks of ICD in A375 MCTS upon treatment with Ir-pbt-Bpa (5 μM) in the dark or upon two-photon irradiation (750 nm, 50 mW, 5 min). (a) One-(OPM) and two-photon (TPM) excited z-stack confocal laser scanning microscopy upon incubation for 12 h. (b) Release of nuclear high-mobility group box 1 protein into the cell culture supernatant. (c) Release of adenosine triphosphate into the cell culture supernatant. (d) Immunofluorescence confocal laser scanning microscopy stained with a nuclear high-mobility group box 1 protein-specific antibody (red) and 4′,6-diamidino-2-phenylindol (blue). Scale bar: 100 μm.

on these findings, the ability of Ir-pbt-Bpa to trigger ICD inside A375 MCTS upon exposure to two-photon light was studied upon monitoring of the respective hallmarks. The treatment of the MCTS showed highly enhanced levels of HMGB1 upon treatment with Ir-pbt-Bpa in the dark and especially upon irradiation (Fig. 4b). In addition, elevated levels of ATP during the treatment were observed (Fig. 4c). Using immunofluorescence confocal laser scanning microscopy, the translocation of calreticulin was detected upon treatment with Ir-pbt-Bpa as indicated by the red fluorescence in the microscopy images (Fig. 4d). The combination of these findings indicates that Ir-pbt-Bpa can penetrate three-dimensional cell structures, causes a strong cytotoxic effect upon two-photon irradiation, and induces ICD.

The evaluation of ICD *in vivo*

The therapeutic efficiency of the treatment with Ir-pbt-Bpa was further evaluated in B16F10 mice melanoma-bearing female C57BL/6J mice. To study the immunogenic response, a primary and a distant secondary tumor model were established on the same animal. The mice models were randomly divided into four groups (Group 1: control; Group 2: light only; Group 3: Ir-pbt-Bpa only; Group 4: Ir-pbt-Bpa + light). Only the primary tumor was intratumorally injected with Ir-pbt-Bpa (3 mg kg^{-1}) and exposed to two-photon irradiation (750 nm, 50 mW, 5 min) 4 h after the administration of the compound (Fig. 5a). While the primary and distant secondary tumors grew exponentially upon treatment with Ir-pbt-Bpa in the dark, a strong tumor growth inhibition effect upon treatment with Ir-pbt-Bpa and exposure to light was observed (photographs of tumors: Fig. 5b, tumor growth inhibition of primary tumor: Fig. 5c, tumor growth inhibition of distant secondary tumor: Fig. 5d). The tumor volume of the primary tumor as well as the distant tumor shrank drastically, indicative of the combined photodynamic and immunotherapeutic effect. A histological examination of the secondary distant tumorous tissue showed severe cellular damage upon treatment with Ir-pbt-Bpa and exposure to irradiation, verifying the immunotherapeutic effect of the treatment (Fig. 5f). Importantly, the mice behave normally without any signs of pain, stress, or discomfort and did not change their body weight (Fig. 5e). In agreement, no histological damage was observed in the major organs of the animal model (Fig. S33†), indicative of the high biocompatibility of the treatment.

The immunogenic response inside the animal model upon treatment with Ir-pbt-Bpa was further investigated. Flow cytometry analysis of the lymph nodes on day 7 demonstrated the enhanced maturation of dendritic cells ($CD45^+$ $CD11c^+$ $CD80^+$ $CD86^+$ cells) upon treatment with Ir-pbt-Bpa and

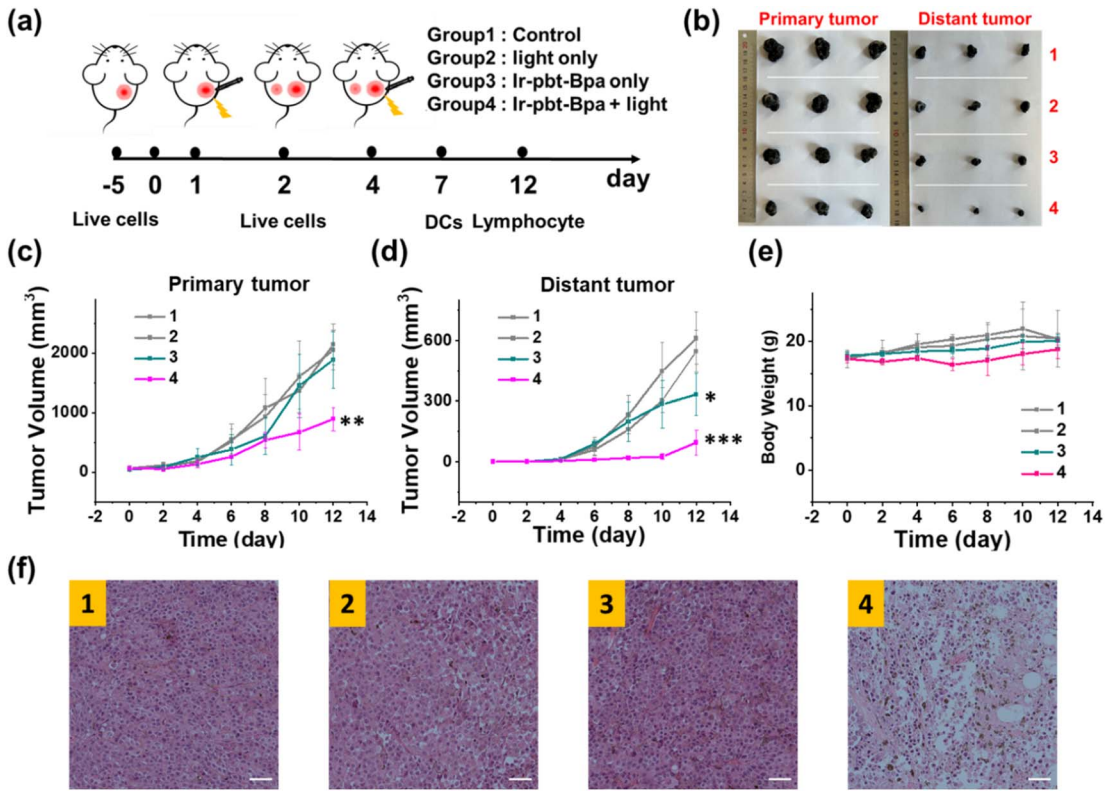

Fig. 5 The treatment of mice models. Evaluation of the treatment of mice models with primary and distant B16F10 mice melanoma tumors upon intratumor injection of Ir-pbt-Bpa (3 mg kg^{-1}) into the primary tumor and exposure to two-photon irradiation (750 nm, 50 mW, 5 min). (a) Schematic timeline of the treatment. (b) Photographs of the collected tumors 12 days after the treatment. (c) Change in the tumor volume of the primary tumor upon treatment. (d) Change in the tumor volume of the secondary tumor upon treatment. (e) Change of the weight of the animal models. (f) Histological examination of the secondary tumor with a hematoxylin and eosin stain 12 days after the treatment. (1) Control; (2) light only; (3) Ir-pbt-Bpa only; (4) Ir-pbt-Bpa + light. ***P < 0.001, **P < 0.01 and *P < 0.05, in comparison to control.

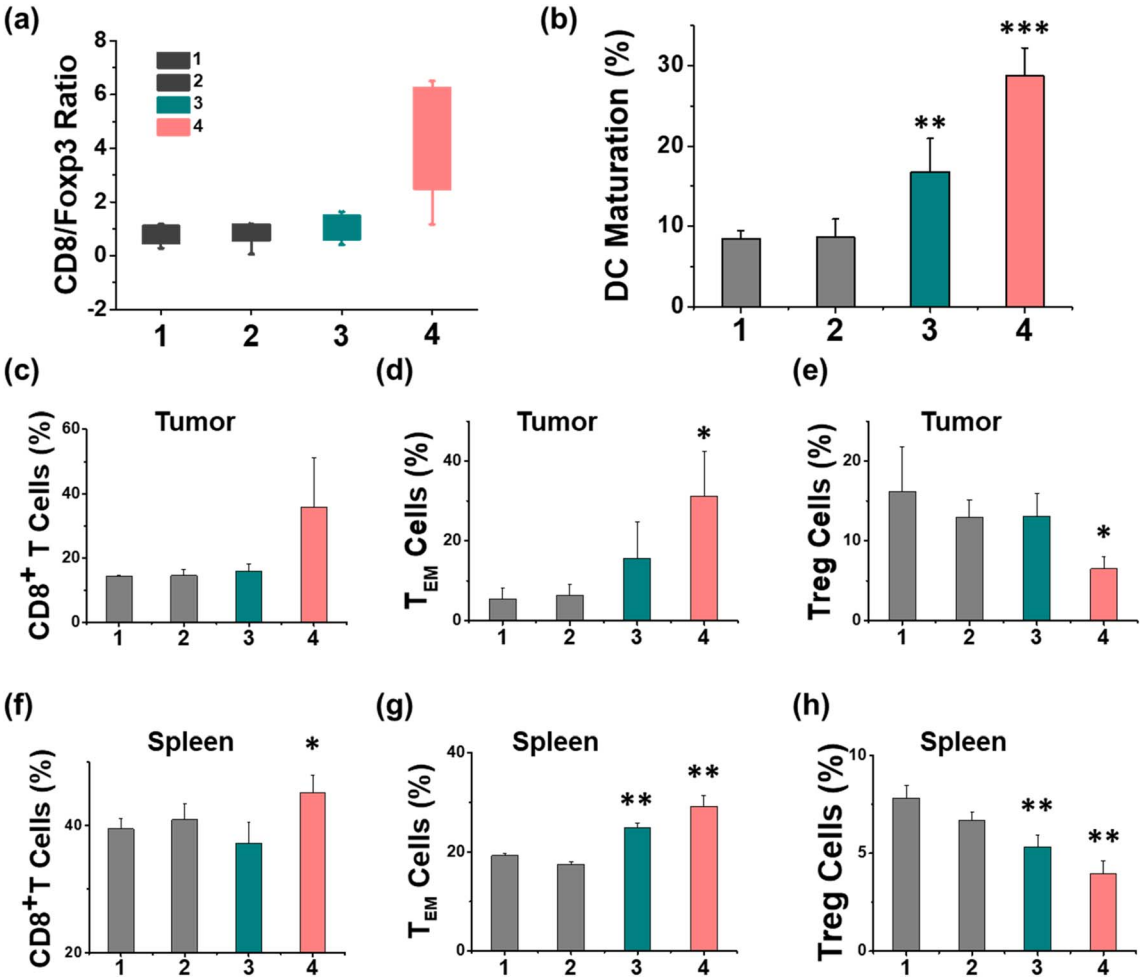

Fig. 6 The immunogenic effect of the treatment of B16F10-bearing mice. Evaluation of the immunogenic effect of the treatment of B16F10-bearing mice by flow cytometry upon intratumor injection of Ir-pbt-Bpa (3 mg kg^{-1}) into the primary tumor and exposure to two-photon irradiation (750 nm, 50 mW, 5 min). (a) Determination of the CD8/Foxp3 ratio in the tumors. (b) Percentages of matured dendritic cells in the lymph nodes on day 7. (c–h) Percentages of $CD8^+$ T cells, effector memory T cells (T_{EM}), and regulatory T cells (T_{reg}) in the primary tumor or the spleen. Mean ± standard deviation ($n = 3$). (1) Control; (2) light only; (3) Ir-pbt-Bpa only; (4) Ir-pbt-Bpa + light. ***$P < 0.001$, **$P < 0.01$ and *$P < 0.05$, in comparison to control.

exposure to irradiation (Fig. 6b and S34†). Followingly, the primary tumorous tissue and spleen tissue were analysed on day 12 after the treatment towards immunogenic effects. The tumor tissue demonstrated an augmentation of cytotoxic $CD8^+$ T cells that are directly responsible for the eradication of cancer cells (Fig. 6c and S35†). Despite the presence of cytotoxic T cells, the immune response could be hampered through the interactions of regulatory T cells ($CD3^+$ $CD4^+$ $CD25^+$ $Foxp3^+$ cells). The treatment with Ir-pbt-Bpa and exposure to irradiation caused a reduction of regulatory T cells, allowing for inhibition of the immune suppressive properties of the tumor (Fig. 6e and S36†). These findings are further represented through the cytotoxic CD8/immune-regulating Foxp3 ratio (Fig. 6a). Using immunofluorescence confocal laser scanning microscopy, the immune infiltration of CD8 and Foxp3 was visualized (Fig. S37†). The combination of this observation indicates that the treatment with Ir-pbt-Bpa and exposure to irradiation caused a strong immune response through the maturation of dendritic cells as well as the reprogramming of tumor immune-suppressive microenvironment, allowing for an enhanced immune response. To investigate the durability of the immunogenic effect, the presence of effector memory T cells ($CD3^+$ $CD8^+$ $CD44^+$ $CD62^-$ cells) was studied. Promisingly, the levels of effector memory T cells were highly enhanced upon treatment with Ir-pbt-Bpa and exposure to light (Fig. 6d and S38†), indicative of a long-lasting immune response inside the animal model. Notably, the same trends for these lymphocytes were observed in the spleen of the mice (Fig. 6f–h and S39–41†). Overall, these findings indicate a strong and long-lasting immunogenic effect upon treatment with Ir-pbt-Bpa by two-photon photodynamic immunotherapy.

Conclusions

In summary, this study reports on the synthesis and in-depth biological evaluation of the iridium(III) complex Ir-pbt-Bpa,

which induces in melanoma cancer cells a combination of localized generation of reactive oxygen species and systemic induction of an immune response upon light irradiation. The compound is primarily localized in the mitochondria and was found, upon light irradiation, to produce oxidative stress, causing cell death through a combination of ferroptosis and immunogenic cell death. Ir-pbt-Bpa demonstrated a strong phototoxic effect in various cancer cell lines, including challenging to treat melanoma cells, as well as multicellular tumor spheroids. Based on the two-photon absorption of our metal complex, it could be excited with the long wavelength in the near-infrared region, ensuring a deep tissue penetration of the light and therefore possibly the treatment of deep-seated tumors.

Based on these promising characteristics, the biological properties of Ir-pbt-Bpa were further studied in an animal model with a primary and distant melanoma tumor. While the compound and the light were only exposed at the primary tumor site, a strong tumor growth inhibition effect in both tumors was observed. Immunogenic studies in the animal model indicated the enhanced maturation of dendritic cells, the remission of the tumor immunosuppressive microenvironment, and the generation of long-lasting memory immune cells. These findings suggest that Ir-pbt-Bpa can therapeutically intervene in tumor-bearing mice through the localized generation of reactive oxygen species by deep-penetrating two-photon photodynamic therapy and the systemic induction of an immune response in the animal model by immunotherapy. Treating a large number of cancer monolayer cells with two-photon irradiation is very difficult. For this reason, most of the biological studies undertaken were performed using 405 nm irradiation while MCTS and *in vivo* data were collected using two-photon irradiation (750 nm).

As the treatment of melanoma remains challenging in the clinics, in particular, due to high tendencies for drug resistance and quick development of metastasis, the combination of photodynamic therapy and immunotherapy described in this study could present a therapeutic alternative. This therapeutic strategy could open new avenues for the treatment of other challenging forms of cancer.

Statistical analysis

The significance of several experimental results was analyzed by using the analysis of *T*-test. Probabilities $p < 0.05$ (*) and $p < 0.01$ (**), ***$P < 0.001$ were marked in figures and 0.05 was chosen as the significance level.

Data availability

ESI† is available and includes the synthesis and characterization of Ir-pbt-Bpa, the detection of cellular ROS levels, lipid peroxides, ferroptosis, and immunogenic cell death upon excitation with one- or two-photon light, the experimental vaccine of ICD *in vivo*.

Author contributions

H. Chao and G. Gasser oversaw and designed all experiments; L. W. synthesized the complex; L. Wang, F. Wei, L. Xie, and Z. Chen performed the photodynamic experiments in the solution and in the cancer cells; L. Wang and Z. Chen performed the animal experiments; L. Wang, J. Karges, G. Gasser and H. Chao analyzed the data and wrote the manuscript. All authors discussed the results and commented on and proofread the manuscript.

Conflicts of interest

The authors declare no competing interests.

Acknowledgements

This research was supported by the National Natural Science Foundation of China (No. 22120102002), the Science and Technology Innovation Program of Hunan Province of China (No. 2021RC5028), and the Research and Cultivation Fund of Hainan Medical University of China (No. HYPY201902). This work was financially supported by an ERC Consolidator Grant PhotoMedMet to G. G. (GA 681679), which has received support under the program "Investissements d'Avenir" launched by the French Government and implemented by the ANR with the reference ANR-10-IDEX-0001-02 PSL (G. G.).

Notes and references

1 L. Peng, M. Wang, Y. Chu, L. Zhang, J. Niu, H. Shao, T. Yuan, Z. Jiang, J. Gao and X. Ning, *Sci. Adv.*, 2020, **6**, e2735.
2 M. Singh, C. Vianden, M. J. Cantwell, Z. Dai, Z. Xiao, M. Sharma, H. Khong, A. R. Jaiswal, F. Faak, Y. Hailemichael, L. M. E. Janssen, U. Bharadwaj, M. A. Curran, A. Diab, R. L. Bassett, D. J. Tweardy, P. Hwu and W. W. Overwijk, *Nat. Commun.*, 2017, **8**, 1447–1456.
3 A. Testori, P. Rutkowski, J. Marsden, L. Bastholt, V. Chiarion-Sileni, A. Hauschild and A. M. M. Eggermont, *Ann. Oncol.*, 2009, **20**, 22–29.
4 L. Zhou, H. Zheng, S. Wang, F. Zhou, B. Lei and Q. Zhang, *Biomaterials*, 2020, **262**, 120300.
5 R. A. Akasov, N. V. Sholina, D. A. Khochenkov, A. V. Alova, P. V. Gorelkin, A. S. Erofeev, A. N. Generalova and E. V. Khaydukov, *Sci. Rep.*, 2019, **9**, 9679.
6 L. M. Davids and B. Kleemann, *Cancer Treat. Rev.*, 2011, **37**, 465–475.
7 L. M. Lifshits, J. A. Roque, P. Konda, S. Monro, H. D. Cole, D. von Dohlen, S. Kim, G. Deep, R. P. Thummel, C. G. Cameron, S. Gujar and S. A. McFarland, *Chem. Sci.*, 2020, **11**, 11740–11762.
8 S. Monro, K. L. Colon, H. Yin, J. Roque, P. Konda, S. Gujar, R. P. Thummel, L. Lilge, C. G. Cameron and S. A. McFarland, *Chem. Rev.*, 2019, **119**, 797–828.
9 D. van Straten, V. Mashayekhi, H. S. de Bruijn, S. Oliveira and D. J. Robinson, *Cancers*, 2017, **9**, 19.

10 J. Li, H. Ou and D. Ding, *Chem. Res. Chin. Univ.*, 2021, **37**, 83–89.
11 S. Zhang, J. Wang, Z. Kong, X. Sun, Z. He, B. Sun, C. Luo and J. Sun, *Biomaterials*, 2022, **282**, 121433.
12 R. Alzeibak, T. A. Mishchenko, N. Y. Shilyagina, I. V. Balalaeva, M. V. Vedunova and D. V. Krysko, *J. Immunother. Cancer*, 2021, **9**, e001926.
13 J. Li, Y. Luo and K. Pu, *Angew. Chem., Int. Ed.*, 2021, **60**, 12682–12705.
14 S. Sen, M. Won, M. S. Levine, Y. Noh, A. C. Sedgwick, J. S. Kim, J. L. Sessler and J. F. Arambula, *Chem. Soc. Rev.*, 2022, **51**, 1212–1233.
15 J. He, Y. Wang, M. A. Missinato, E. Onuoha, L. A. Perkins, S. C. Watkins, C. M. St Croix, M. Tsang and M. P. Bruchez, *Nat. Methods*, 2016, **13**, 263–268.
16 H. Xu, D. Lin, B. Zhang, Y. Huo, S. Lin, C. Liu, C. Chen and C. Wang, *Drug Delivery*, 2020, **27**, 378–386.
17 X. Cai, K. Wang, W. Ma, Y. Yang, G. Chen, H. Fu, C. Cui, Z. Yu and X. Wang, *J. Nanobiotechnol.*, 2021, **19**, 254.
18 X. Han, H. Li, Y. Jiang, H. Wang, X. Li, J. Kou, Y. Zheng, Z. Liu, H. Li, J. Li, D. Dou, Y. Wang, Y. Tian and L. Yang, *Cell Death Dis.*, 2017, **8**, e2864.
19 C. T. Inglut, Y. Baglo, B. Liang, Y. Cheema, J. Stabile, G. F. Woodworth and H. Huang, *J. Clin. Med.*, 2019, **8**, 1269.
20 Y. Li, X. Liu, X. Zhang, W. Pan, N. Li and B. Tang, *Chem. Commun.*, 2021, **57**, 12087–12097.
21 Y. Wu, S. Li, Y. Chen, W. He and Z. Guo, *Chem. Sci.*, 2022, **13**, 5085–5106.
22 J. Li and T. Chen, *Coord. Chem. Rev.*, 2020, **418**, 213355.
23 L. Gourdon, K. Cariou and G. Gasser, *Chem. Soc. Rev.*, 2022, **51**, 1167–1195.
24 V. Fernandez-Moreira, F. L. Thorp-Greenwood and M. P. Coogan, *Chem. Commun.*, 2010, **46**, 186–202.
25 V. Balzani, G. Bergamini, F. Marchioni and P. Ceroni, *Coord. Chem. Rev.*, 2006, **250**, 1254–1266.
26 P. Konda, L. M. Lifshits, J. A. Roque, H. D. Cole, C. G. Cameron, S. A. McFarland and S. Gujar, *OncoImmunology*, 2021, **10**, e1863626.
27 Z. Deng, N. Wang, Y. Liu, Z. Xu, Z. Wang, T. C. Lau and G. Zhu, *J. Am. Chem. Soc.*, 2020, **142**, 7803–7812.
28 B. Englinger, C. Pirker, P. Heffeter, A. Terenzi, C. R. Kowol, B. K. Keppler and W. Berger, Metal drugs and the anticancer immune response, *Chem. Rev.*, 2019, **119**, 1519–1624.
29 V. Novohradsky, J. Pracharova, J. Kasparkova, C. Imberti, H. E. Bridgewater, P. J. Sadler and V. Brabec, *Inorg. Chem. Front.*, 2020, **7**, 4150–4159.
30 D. Wei, Y. Huang, B. Wang, L. Ma, J. Karges and H. Xiao, *Angew. Chem., Int. Ed.*, 2022, **61**, e202201486.
31 X. Su, W. Wang, Q. Cao, H. Zhang, B. Liu, Y. Ling, X. Zhou and Z. Mao, *Angew. Chem., Int. Ed.*, 2021, **60**, e202115800.
32 G. Vigueras, L. Markova, V. Novohradsky, A. Marco, N. Cutillas, H. Kostrhunova, J. Kasparkova, J. Ruiz and V. Brabec, *Inorg. Chem. Front.*, 2021, **8**, 4696–4711.
33 J. Karges, *Angew. Chem., Int. Ed.*, 2022, **61**, e202112236.
34 S. Kuang, L. Sun, X. Zhang, X. Liao, T. W. Rees, L. Zeng, Y. Chen, X. Zhang, L. Ji and H. Chao, *Angew. Chem., Int. Ed.*, 2020, **59**, 20697–20703.
35 X. Tian, Y. Zhu, M. Zhang, L. Luo, J. Wu, H. Zhou, L. Guan, G. Battaglia and Y. Tian, *Chem. Commun.*, 2017, **53**, 3303–3306.
36 Y. Chen, R. Guan, C. Zhang, J. Huang, L. Ji and H. Chao, *Coord. Chem. Rev.*, 2016, **310**, 16–40.
37 L. K. McKenzie, H. E. Bryant and J. A. Weinstein, *Coord. Chem. Rev.*, 2019, **379**, 2–29.
38 J. Karges, S. Kuang, F. Maschietto, O. Blacque, I. Ciofini, H. Chao and G. Gasser, *Nat. Commun.*, 2020, **11**, 3262.
39 X. Zhao, J. Liu, J. Fan, H. Chao and X. Peng, *Chem. Soc. Rev.*, 2021, **50**, 4185–4219.
40 L. Wang, R. Guan, L. Xie, X. Liao, K. Xiong, T. W. Rees, Y. Chen, L. Ji and H. Chao, *Angew. Chem., Int. Ed.*, 2021, **60**, 4657–4665.
41 B. Gu, W. Wu, G. Xu, G. Feng, F. Yin, P. Chong, J. Qu, K. Yong and B. Liu, *Adv. Mater.*, 2017, **29**, 1701076.
42 T. De Raedt, Z. Walton, J. L. Yecies, D. Li, Y. Chen, C. F. Malone, O. Maertens, S. M. Jeong, R. T. Bronson, V. Lebleu, R. Kalluri, E. Normant, M. C. Haigis, B. D. Manning, K. Wong, K. F. Macleod and K. Cichowski, *Cancer Cell*, 2011, **20**, 400–413.
43 C. Chen, X. Ni, S. Jia, Y. Liang, X. Wu, D. Kong and D. Ding, *Adv. Mater.*, 2019, **31**, 1904914.
44 A. Chen, L. Burr and M. A. McGuckin, *Clin. Transl. Immunol.*, 2018, **7**, e1019.
45 A. Q. Sukkurwala, S. Adjemian, L. Senovilla, M. Michaud, S. Spaggiari, E. Vacchelli, E. E. Baracco, L. Galluzzi, L. Zitvogel, O. Kepp and G. Kroemer, *OncoImmunology*, 2014, **3**, e28473.
46 A. D. Garg, D. V. Krysko, T. Verfaillie, A. Kaczmarek, G. B. Ferreira, T. Marysael, N. Rubio, M. Firczuk, C. Mathieu, A. J. M. Roebroek, W. Annaert, J. Golab, P. de Witte, P. Vandenabeele and P. Agostinis, *EMBO J.*, 2012, **31**, 1062–1079.
47 J. Li, Y. Fang, Y. Zhang, H. Wang, Z. Yang and D. Ding, *Adv. Mater.*, 2021, **33**, e2008518.
48 M. J. R. Tham, M. V. Babak and W. H. Ang, *Angew. Chem., Int. Ed.*, 2020, **59**, 19070–19078.
49 S. Sen, S. Hufnagel, E. Y. Maier, I. Aguilar, J. Selvakumar, J. E. DeVore, V. M. Lynch, K. Arumugam, Z. Cui, J. L. Sessler and J. F. Arambula, *J. Am. Chem. Soc.*, 2020, **142**, 20536–20541.
50 W. Li, J. Yang, L. Luo, M. Jiang, B. Qin, H. Yin, C. Zhu, X. Yuan, J. Zhang, Z. Luo, Y. Du, Q. Li, Y. Lou, Y. Qiu and I. You, *Nat. Commun.*, 2019, **10**, 3349.
51 W. Yin, F. Liao, M. Chen, X. Qin, H. Lai, Y. Lin and D. Yao, *Aging*, 2021, **13**, 16713–16732.
52 D. Jia, J. Zheng, Y. Zhou, J. Jia, X. Ye, B. Zhou, X. Chen, Y. Mo and J. Wang, *J. Inflammation Res.*, 2021, **14**, 5393–5401.
53 H. Zhang, T. Deng, R. Liu, T. Ning, H. Yang, D. Liu, Q. Zhang, D. Lin, S. Ge, M. Bai, X. Wang, L. Zhang, H. Li, Y. Yang, Z. Ji, H. Wang, G. Ying and Y. Ba, *Mol. Cancer*, 2020, **19**, 43.
54 W. Wang, M. Green, J. E. Choi, M. Gijon, P. D. Kennedy, J. K. Johnson, P. Liao, X. Lang, I. Kryczek, A. Sell, H. Xia,

J. Zhou, G. Li, J. Li, W. Li, S. Wei, L. Vatan, H. Zhang, W. Szeliga, W. Gu, R. Liu, T. S. Lawrence, C. Lamb, Y. Tanno, M. Cieslik, E. Stone, G. Georgiou, T. Chan, A. Chinnaiyan and W. Zou, *Nature*, 2019, **569**, 270–274.

55 Y. Xu, Y. Guo, C. Zhang, M. Zhan, L. Jia, S. Song, C. Jiang, M. Shen and X. Shi, *ACS Nano*, 2022, **16**, 984–996.

56 W. Wang, Y. Ling, Y. Zhong, Z. Li, C. Tan and Z. Mao, *Angew. Chem., Int. Ed.*, 2021, **61**, e202115247.

57 Z. Tang, Z. Huang, Y. Huang, Y. Chen, M. Huang, H. Liu, Q. Ye, J. Zhao and B. Jia, *Front. Cell Dev. Biol.*, 2021, **9**, 765859.

58 I. Efimova, E. Catanzaro, L. Van der Meeren, V. D. Turubanova, H. Hammad, T. A. Mishchenko, M. V. Vedunova, C. Fimognari, C. Bachert, F. Coppieters, S. Lefever, A. G. Skirtach, O. Krysko and D. V. Krysko, *J. Immunother. Cancer.*, 2020, **8**, e001369.

59 J. Zheng and M. Conrad, *Cell Metab.*, 2020, **32**, 920–937.

60 C. Liang, X. Zhang, M. Yang and X. Dong, *Adv. Mater.*, 2019, **31**, e1904197.

61 H. Yuan, Z. Han, Y. Chen, F. Qi, H. Fang, Z. Guo, S. Zhang and W. He, *Angew. Chem., Int. Ed.*, 2021, **60**, 8174–8181.

62 D. Tang, O. Kepp and G. Kroemer, *Oncoimmunology*, 2020, **10**, 1862949.